International Journal of Multiphase Flow 36 (2010) 193–201

Contents lists available at ScienceDirect

International Journal of Multiphase Flow

journal homepage: www.elsevier.com/locate/ijmulflow

Measuring particle size distribution using LED-illumination

Yan Jiang [a,b,*], Hong Young Jeon [c], Lei Tian [b], Loren E. Bode [b]

[a] School of Transportation Science and Engineering, BeiHang University, Beijing 100191, China
[b] Department of Agricultural Biological Engineering, University of Illinois at Urbana-Champaign, Urbana, IL 61801, USA
[c] Agricultural Research Service-USDA Wooster, OH 44691, USA

ARTICLE INFO

Article history:
Received 18 August 2009
Received in revised form 22 October 2009
Accepted 4 November 2009
Available online 22 December 2009

Keywords:
LED-illumination
Droplet size distribution
Particle/droplet image analysis
Upper-limit lognormal distribution

ABSTRACT

A particle/droplet image analysis (PDIA) system employing LED-illumination was designed. Freezing the moving droplets using high speed camera instead of stroboscopic illumination, the system had no requirement to synchronize the backlight and the camera. It featured low cost, low power consumption and simple optical configuration in comparison to laser-based systems. Only focused droplets in images were counted. Given the sample size of the system was relatively small, an upper-limit lognormal distribution was used to fit the actual data to represent the spray patterns. The accuracy of the diameter measurement was verified using precisely manufactured balls. Comparisons with two laser-based systems were given and the system's capacity to distinct spray patterns were demonstrated in nozzle classification experiments.

1. Introduction

Droplet size measurement was utilized in various applications, including engine industry, agriculture and atmospheric studies (Benayahu et al., 1995; Berthoumieu et al., 1999; Humeau et al., 2007; Womac et al., 2001; Jeon et al., 2004). Huimin (2000) classified droplet sizing techniques into mechanical methods, electrical methods, optical methods and acoustical methods. Mechanical methods and most early electrical methods interrupted the spray pattern and were unappealing in recent decades. Hot-wire method was based on the observation that the droplet impinging a heated platinum wire caused change in resistance (Mahler and Magnus, 1984). Despite being an intrusive technique, this method created very limited disturbance to the spray. Optical methods were all non-intrusive to the spray pattern. Laser-scattering method analyzed the scattered light at a specific angle bias the incident light. When a laser beam was incident with a particle, the reflection and refraction light intersected and formed fringes. A simple relationship between fringe patterns and droplet sizes was presented by Ragucci et al. (1990). Phase-Doppler Anemometry (PDA) detected phase differences in the incident and scattered light (Buchhave and Von Benzon, 1996). Another solution for droplet sizing was particle/droplet image analysis (PDIA) that captured and processed the microscopic image of the spray (Berthoumieu et al., 1999). Laser-based optical methods had been established as standard techniques for droplet size measurement (ASAE Standard S-572, 2004). However, such commercially available devices were rather expensive and required complicated optic alignment.

A PDIA system using ultra bright LED as illumination source was designed in the work. Replacing the laser with LED reduced the cost significantly. Unlike other PDIA methods using stroboscopic laser or flash lamp, the LED array was kept on during the measurement and a high speed camera was used to capture droplets in motion. This removed the requirement to strobe the LED and synchronize the backlight with the camera. The LED array was placed on the opposite side of the camera without a diffuser. Thus the optic alignment of the vision system was rather simple. In addition, a 12 V lead–acid battery was sufficient to power the whole system due to its low energy consumption (<10 w).

A data-processing program was designed to extract the well-focused droplets from the image and calculate the size distribution. Measurements were done at five positions in the spray and combined for a representative distribution as a result that the volume distribution was not homogenous in the spray fan. The system was unable to collect representative samples to generate a smooth curve in short time due to the small depth of view (DOV) of the camera and the limitation of the camera frame rate. Thus an upper-limit lognormal distribution (ULLN) was used to fit the actual curve.

The system configuration and the data-processing program were presented in the next two sections. Experimental results and discussions were provided in Section 4, including the

* Corresponding author. Address: Department of Agricultural Biological Engineering, University of Illinois at Urbana-Champaign, 1304 W. Pennsylvania Avenue, Urbana, IL 61801, USA. Tel.: +1 217 333 7534; fax: +1 217 244 0323.
E-mail addresses: jiangyanzuzu@msn.com (Y. Jiang), hongyoung.jeon@ars.usda.gov (H.Y. Jeon), lei-tian@illinois.edu (L. Tian), bode@illinois.edu (L.E. Bode).

0301-9322/$ - see front matter © 2009 Elsevier Ltd. All rights reserved.
doi:10.1016/j.ijmultiphaseflow.2009.11.004

determination of the sample size, the investigation of the measurement position's influence on the distribution, the verification of the size measurement accuracy using precision balls, comparisons with two laser-based systems (the Malvern system and the Oxford Lasers VisiSizer system) and a nozzle classification test. Finally, the conclusion and future work were given.

2. System configuration

The system (Fig. 1) consisted of a high speed CCD camera (701b, Unibrain SA, Athens, Greece), an 6-by-5 array of ultra bright LED (Fig. 2) (Super Bright LEDs Inc., luminous intensity 18000 mcd, view angle 30°, wavelength in CIE 1931 $x = 0.277$, $y = 0.277$), and a PC to control the camera and process images. The total cost of the system was around $2 k.

The camera worked at a frame rate up to 15 fps and communicated with the computer via IEEE 1394 fire-wire. It was equipped with a monochrome CCD (ICX-205AL, Pixel size: 4.65 μm × 4.65 μm, Sony Co., Tokyo, Japan). Four 5-mm spacers (Edmund optics, Barrington, NJ, USA) were installed between the camera and telescope lens (focal length range: 12.5–75 mm, Navitar TV Zoom Lens, F 1.8, Japan) to increase the magnification of the camera view at the focus distance. The size of the field of view (FOV) was approximately 10.6 mm (h) × 7.9 mm (w) and the depth of field (DOF) was approximately ±1.3 mm. The resolution of the output image was 640 × 480 and the pixel size in the image was approximately 16.5 μm per pixel. The FOV was horizontally 20 cm away from the camera body (focus distance) and the vertical distance D_1 from the FOV to the nozzle orifice was 40 cm. Large D_1 was likely to result in droplets impinging on the lens due to the small focus distance, whereas droplets may not break up completely if D_1 was small.

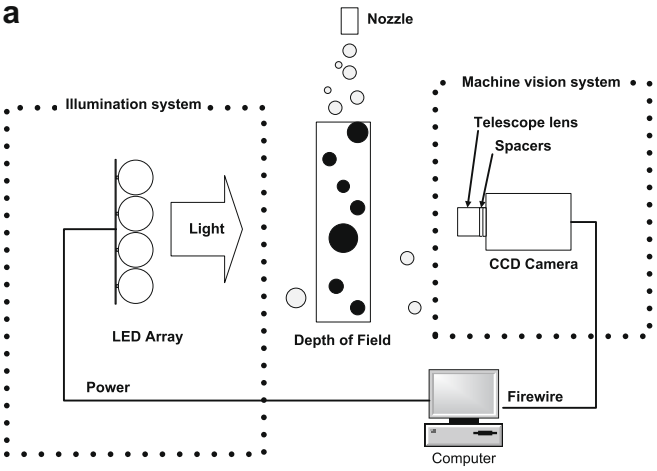

Fig. 1. System configuration.

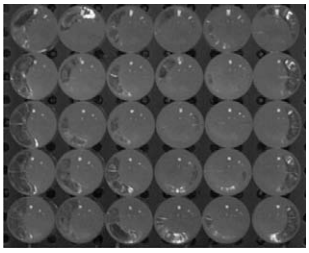

Fig. 2. 6-by-5 LED array.

The shutter speed and gain of camera were set by the computer. Considering the pixel size, the shutter speed was set one micron second so that the movement of a droplet was smaller than one pixel during the exposure time. The gain value was selected carefully to control the brightness of the image. On one hand, gain value should allow sufficient contrast in the image to distinguish droplets from background. On the other hand, excessive gain value may erode droplets' edge and introduce noises into the image. A captured image is showed in Fig. 3a.

3. Droplet sizing processing program

The data-processing program was developed using Microsoft Visual C++ 2005 (Microsoft Co., Redmond, WA, USA) and Fire-I API (Application Programming Interface, Unibrain Co. Ltd., Greece). It processed captured images and displayed the real-time results (Fig. 4a). The camera saved images in either buffer or files. Since the total processing time was approximately 15 ms for a single image, the system could run at a full frame rate of 15 fps when images were read from buffer. However, only five images could be processed when images were saved as files. As shown in Fig. 4b, the core component of the droplet sizing processing program consists of real-time image processing and curve fitting post processing.

3.1. Segmentation by background subtraction

Uniform illumination was important to the following image processing and using large view angle LED could improve the image quality significantly. However, slight difference still existed in the background. Given the LED illumination was stable after it warmed up, a background image was captured and saved in the memory at the beginning of the measurement. Every followed image was subtracted from it (Fig. 3b) and then segmented using a threshold of 30, which was determined by visual analysis. After that, a 3-by-3 medium filter was applied to the resultant image. It should be noted that the size of the medium filtering window was relatively small to avoid eliminating small droplets.

3.2. Grouping

The grouping function clustered pixels as droplets. Each droplet was labeled with a distinct ID and the properties including size and position were also available after grouping. A 2-by-3 window was used to scan the image from left to right and from top to bottom. Given the pixel $P_{2,2}$ in the window was on a droplet, IDs of the four adjacent pixels [$P_{1,1}$, $P_{1,2}$, $P_{1,3}$, $P_{2,1}$] which had been scanned were

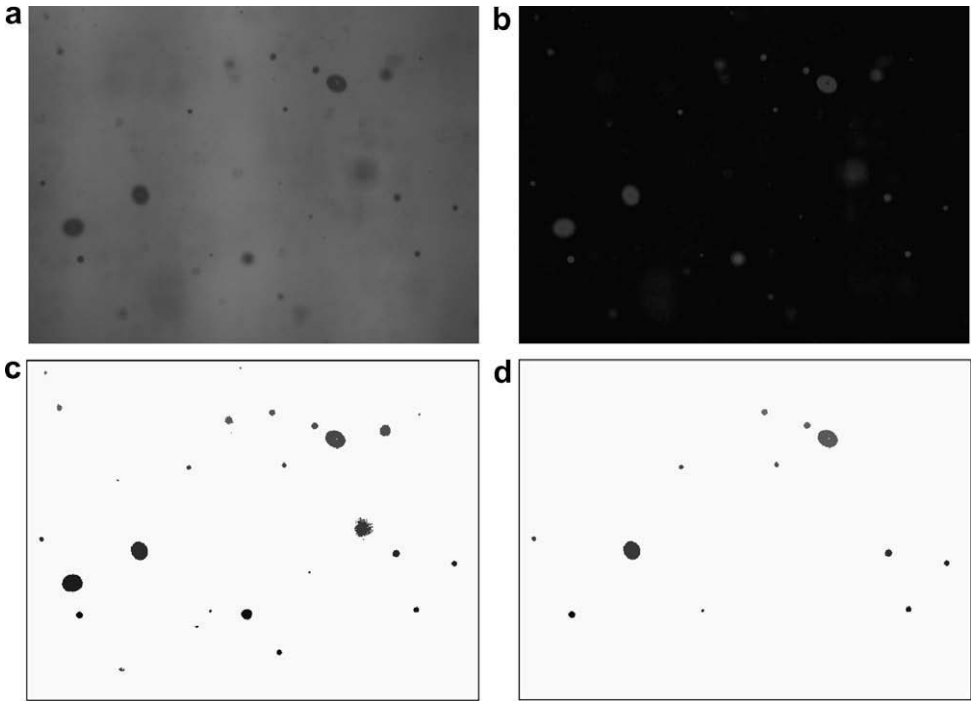

Fig. 3. Image processing results step by step.

collected as dataset D_s and $P_{2,2}$ was set an ID based on one of the following cases.

Case 1 (Fig. 5a): If no ID had been set in D_s, $P_{2,2}$ was on a new droplet and it was set with a new ID (increasing the maximum existing ID by 1).

Case 2 (examples in Fig. 5b–e): If some pixels in D_s were labeled with one ID, $P_{2,2}$ was on the same droplet and set with the ID of this droplet.

Case 3 (Fig. 5f–h): The most complicated situation was that D_s contained different IDs, which implied two previously detected droplets were actually one droplet and connected at $P_{2,2}$. In this case, $P_{2,2}$ was set with the smaller ID and all the pixels with the larger ID were reassigned the smaller ID.

After the grouping step, the assigned IDs were likely not continuous due to case 3. Fig. 3c was the grouping result of Fig. 3b, where each droplet had its pixel value equal to its ID.

3.3. Gradient analysis for focus distinction

A mixture of focused and out-of-focus droplets was expected in the image due to the small DOF of the vision system. Although the very low-contrast droplets that were far from the focal distance had been removed in the segmentation processes, defocused droplets were still unavoidable. These droplets may result in inaccurate measurements. Kashdan et al. (2003) reported that the extent of defocus was related to the size of the droplet and the displacement from the working distance. Droplets eventually became indistinguishable from the background as the displacement from the focal distance increased.

In the gradient analysis, the sharpness of the droplet's edge was calculated using the following equation:

$$y = (X_b - X_t)/X_m = \left[X_b - \left(\sum_{i=1}^{4} D_i\right) \Big/ 4\right] \Big/ X_m \quad (1)$$

where X_b is the background pixel; X_m is the minimum value of the droplet; D_i is the subtraction of first pixel outside the droplet and the second pixel inside the droplet (Fig. 6a); y in Eq. (1) was used to classify a droplet focused or not. The selection of the threshold of y had direct influenced on the measurement results and was determined by visual analysis. Fig. 6b showed an sample image containing both focused and defocused droplets of different sizes. y value of each droplet was listed in Table 1.

Eq. (1) was only applied for droplets larger than 20 pixels in area because the diameter of small droplets was too small to calculate D_i. For these droplets, minimum pixel values were used instead of calculating y.

After defocused droplets were eliminated, the diameter of a focused droplet was calculated using the following equations:

$$D = \sqrt{4A/\pi} \times R_p \quad (2)$$

where A is the pixel number of the droplet in the image; R_p is the real world pixel size (16.5 μm in the system).

Eq. (2) was based on the estimation that droplets were in shape of sphere and it was feasible when the vertical working distance from the nozzle to the measurement volume was sufficient for droplets to break up completely (Berthoumieu et al., 1999).

3.4. ULLN curve fitting

Due to the limitation of the camera frame rate and the small FOV, the system was unable to collect representative samples in short time to output a smooth curve in comparison to PDA or Laser-scattering systems.

Parameters like Dv0.1, Dv0.5 and Dv0.9 that were used to represent the volume distribution in agricultural spraying applications (Womac, 2000) may fluctuate easily if actual data was used. Replacing the actual curve with a upper-limit lognormal (ULLN) distribution may attenuate the undesired effect with the observation that this math model was able to represent various spray patterns (Goering et al., 1978; Mugele and Evans, 1951). The ULLN distribution, which density function was listed in Eq. (3) (Bezdek and Solomon, 1983), featured the following advantageous attributes: (1) it went through the origin; (2) it

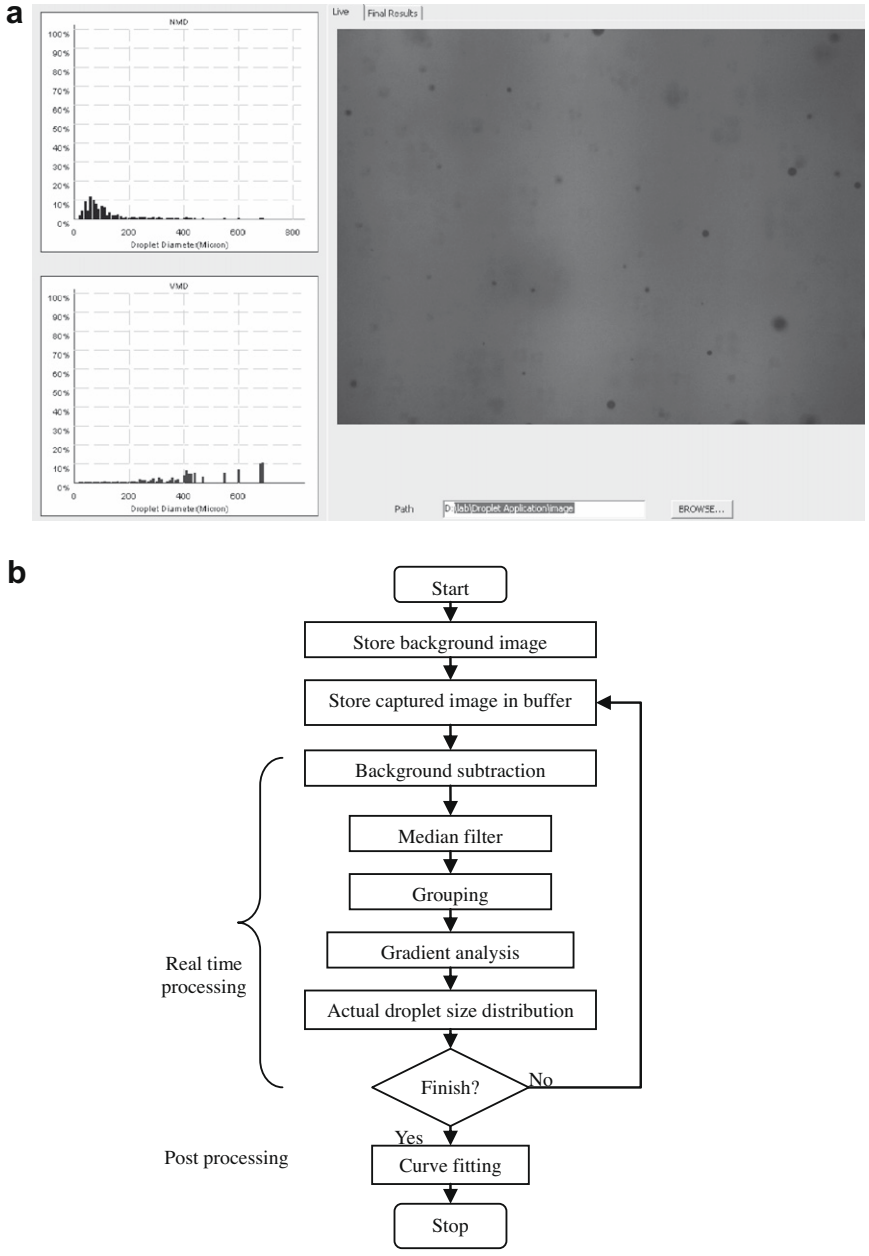

Fig. 4. Program interface and flowchart.

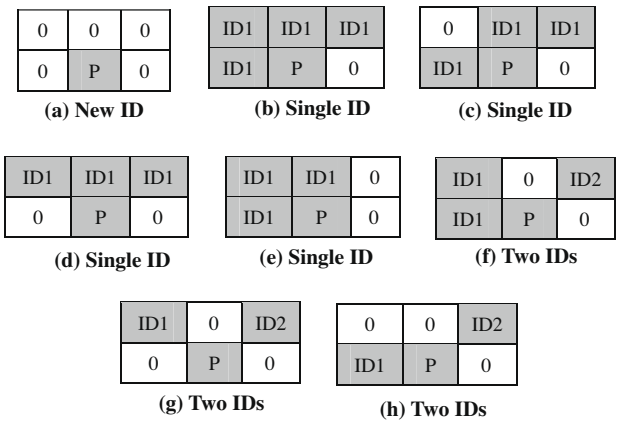

Fig. 5. Pixel grouping.

could represent right skew, left skew, or even two peak distribution by adjusting parameters; (3) it could limit the maximum diameter of the droplets.

$$\frac{\alpha\left\{\exp\left[\frac{(\log\frac{x}{\alpha-x}-\log\mu)^2}{\sigma^2}\right]\right\}^{0.5}}{\sigma x(\alpha-x)\sqrt{2\pi}} \tag{3}$$

Example of using the ULLN distribution to fit an actual curve of a TeeJet 8004vs nozzle was displayed in Fig. 7. The actual curve was measured at the center position in the spray under 344 kPa.

4. Experiments and discussion

4.1. Position's influence on the measurement results

Position's influence on the volume distribution was investigated by measuring at different positions in the spray. Fig. 8a was the re-

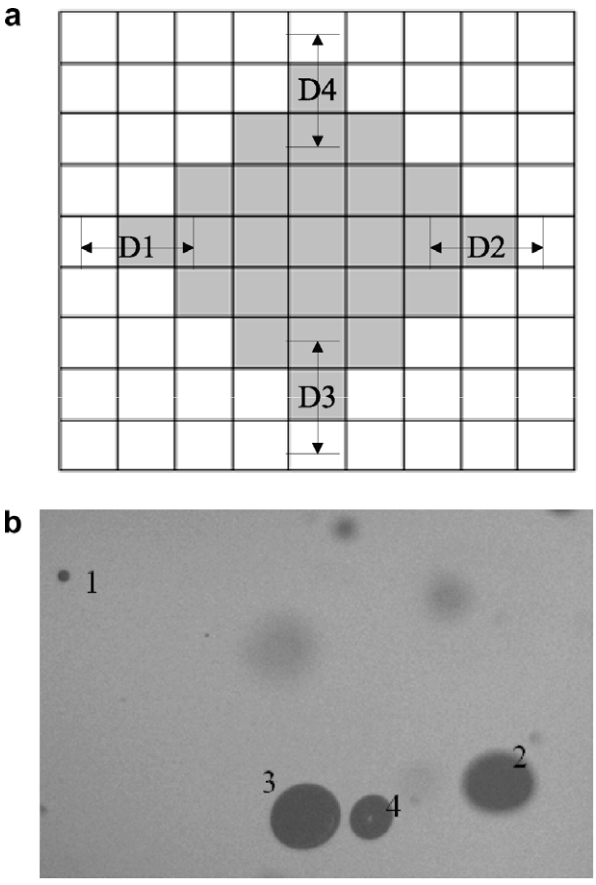

Fig. 6. Focus distinction.

Table 1
Results of focus distinction.

Index	Size (pixel)	X_b	X_t	X_m	y	Focused
1	82	124	81	66	0.65	Yes
2	2278	127	107	70	0.28	No
3	2723	136	93	67	0.65	Yes
4	1124	138	88	71	0.70	Yes

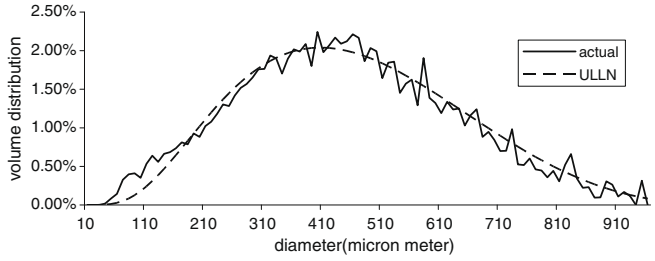

Fig. 7. ULLN curve fitting.

sult at 10 cm left to the center and Fig. 8b was 10 cm right. The curves were narrower and skewed to the small portion in comparison to the center position. This implied the volume distribution was not homogenous in the spray fan. As a result, it was suggested to measure the spray at different positions and combined the results for a representative distribution. Currently, the measurement volume was placed at five positions in the spray: center below the nozzle orifice, 10 cm left and right to the center position, 20 cm left and right to the center position.

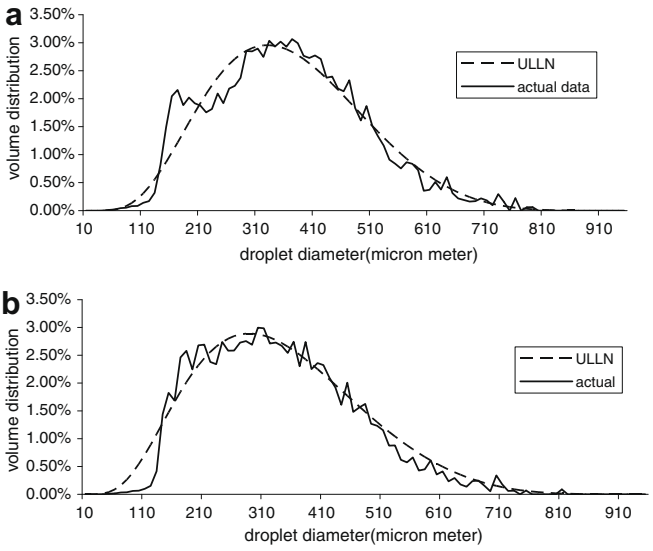

Fig. 8. Distributions at left and right position in the spray.

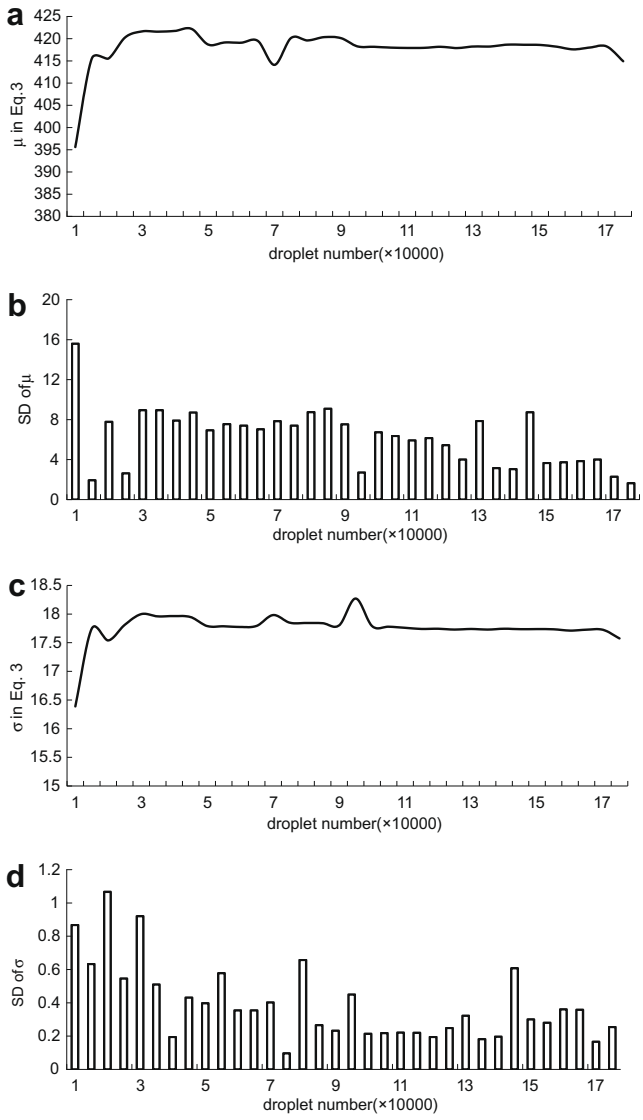

Fig. 9. Curve fitting results at different sample size.

4.2. Determination of the sample size

Measurements were done for different sample sizes to determine how many droplets was sufficient to represent a spray. Results suggested that parameters in the ULLN distribution achieved their steady state after 100,000 droplets were captured (Fig. 9a and c). The test was repeated three times and the stand deviation of these parameters were also displayed in Fig. 9b and d.

4.3. Improvement in the repeatability using curve fitting technique

Measurements results of the same spray pattern were required to be repeatable for a reliable system. Three measurements were conducted using the aforementioned nozzle at 206 kPa (30 psi), and the variance in the Dv0.1, Dv0.5 and Dv0.9 of the actual and fitted curve was compared. Same comparisons were also done at 275 kPa (40 psi) and 344 kPa (50 psi). The improvement in the repeatability using curve fitting technique was significant based on the results in Fig. 10, especially at low pressure which allowed more large droplets. This was reasonable because large droplets shifted the actual curve easily, whereas the curve fitting procedure may attenuate their impact.

4.4. The precision ball test

This test was aimed at verifying the diameter measurement accuracy. An aluminum alloy ball which size was precisely known was fixed between two glass slides and measured. The accuracy of the system was evaluated by comparing its calculated and actual diameter. Three sets of balls with different diameters were involved: (1) 794 μm with grade 200 (tolerance 25 μm) (McMaster, Santa Fe Springs, CA, USA) (Fig. 11a); (2) 498 μm with grade 25 (tolerance 2.5 μm) (Fig. 11b) and (3) 254 μm with grade 24 (tolerance 2.5 μm) (Bal-tec Inc., Los Angeles, CA, USA) (Fig. 11c).

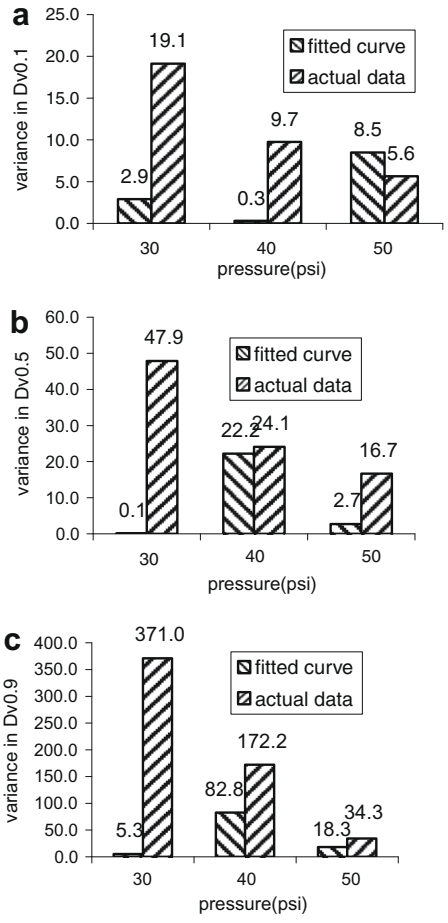

Fig. 10. Variance of volume distribution of actual and fitted curve.

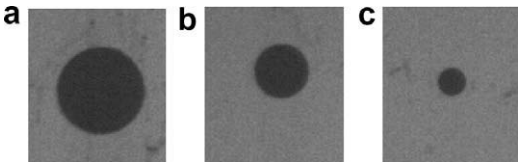

Fig. 11. Images of precision ball.

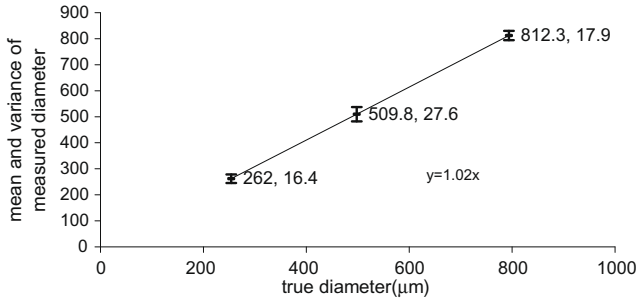

Fig. 12. Measured diameter of precision balls.

Three balls were picked up and 500 image samples were collected for each diameter. Fig. 12 showed the mean diameter and variance of these measurements. The errors between the measured diameter and its true value were 2.3% for 794 μm ball, 2.4% for 498 μm ball and 3.5% for 254 μm ball. A strong linear correlation (coefficient of determination of 1.02) was found between the true diameter and measured mean diameter, thereby implying that the instrument was capable of measuring spheres as large as 800 μm accurately.

Though a new system was required to have its results evaluated by a standard laser system (ASAE Standard S-572 2004), it was difficult for two different systems to have the same numerical results. However, measurements of the same spray pattern should show some extent of similarity. Tests were done to compare the system with Malvern system, Oxford Lasers VisiSizer system to investigate their relations.

4.5. Comparison with laser-based Malvern system

A nozzle (11003XR (TeeJet)) was measured using the two system at three pressures (103 kPa Fig. 13a, 206 kPa Fig. 13b and 310 kPa Fig. 13c) and the results were compared in Fig. 13d and e. The two systems had similarity in that the changes from 206 kPa (30 psi) to 310 kPa (45 psi) was much smaller than that from 103 kPa (15 psi) to 206 kPa (30 psi). However, it could be seen that the pressure change's influence on the distribution was relatively small in the system compared with the Malvern system.

4.6. Comparison with Oxford Lasers system

Similar to the system, the Oxford Lasers VisiSizer was also based on the PDIA principle. High similarity could be found in the measurement result of a 8002XR (TeeJet) nozzle at 289.6 kpa (Fig. 14). Some extent of disagreement was expected due to the different vertical working distances in the two systems.

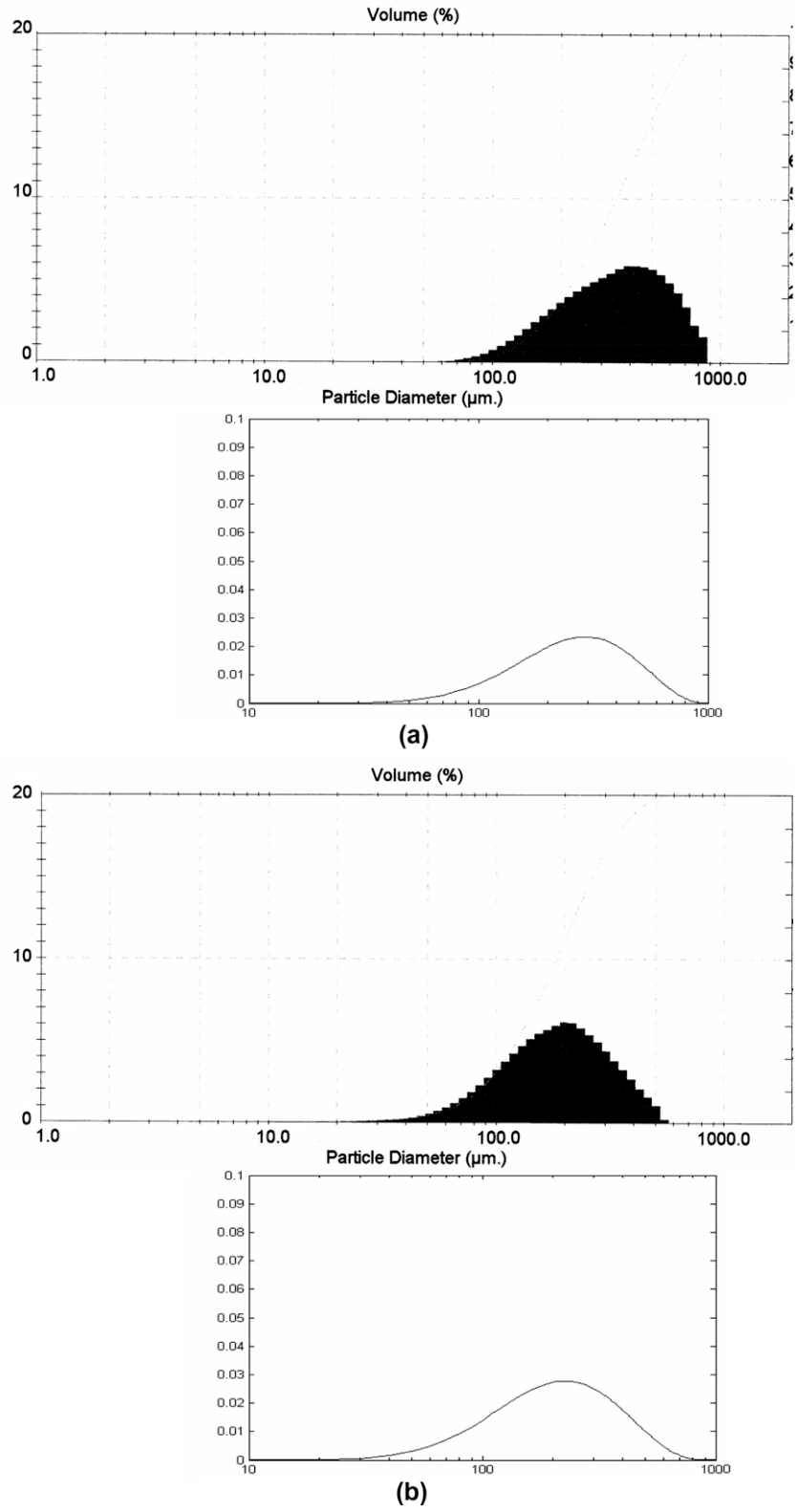

Fig. 13. Comparison with the Malvern system.

4.7. Nozzle classification test

Despite different from other systems in numeric results, the system should distinct spray patterns correctly. A set of nozzles with known spray patterns were measured in the nozzle classification test. Each nozzle was used to generate two types of spray under different pressures according to the manufacturers' catalog (Catalog 50, Teejet, Wheaton, IL, USA) and these distributions covered the range from very fine to very coarse (Table 2). The system classified the spray patterns successfully (Fig. 15).

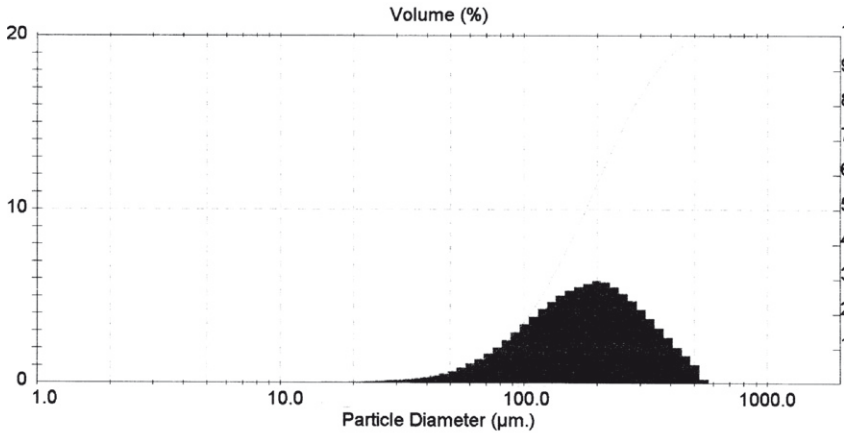

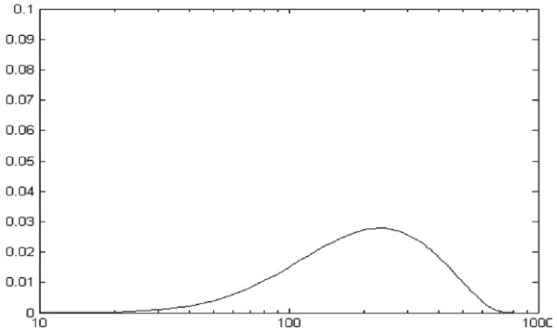

(c)

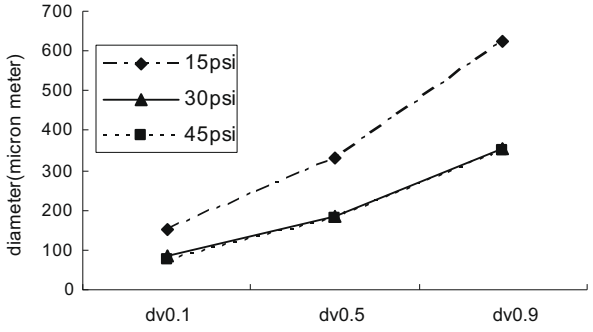

(d) Laser system

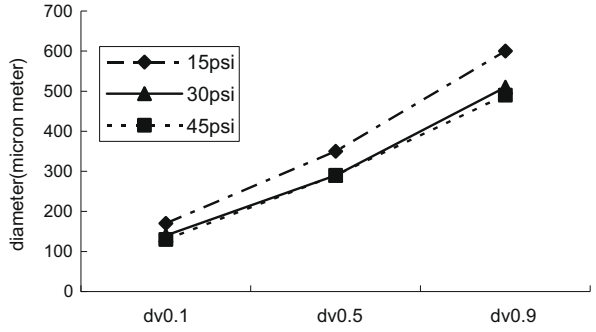

(e) LED system

Fig. 13 (*continued*)

5. Conclusion and discussion

A PDIA system using LED as the illumination source was designed. The minimum of the measurable diameter was 30 μm under the current optical configuration. If it was required to measure small droplets precisely, the minimum of diameter range could be improved by changing magnifier. However, it was difficult for a PDIA-based system to achieve sub-micron accuracy (Huimin, 2000). Thus this work was aimed at providing at a low cost and portable solution with reasonable accuracy for applications where

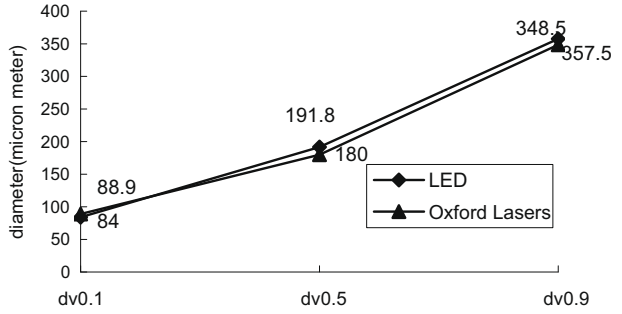

Fig. 14. Comparison with Oxford Lasers VisiSizer system.

Table 2
Classification of the nozzles at different pressure by the manufacturer.

Nozzle type	Pressure (kPa)	Manufacturer's nozzle classification at the operating condition
XR11001	344.74	Very fine
XR11001	206.84	Fine
XR8002	275.79	Fine
XR8002	137.90	Medium
XR8004	275.79	Medium
XR8004	137.90	Course
XR8008	275.79	Course
XR8008	137.90	Very course

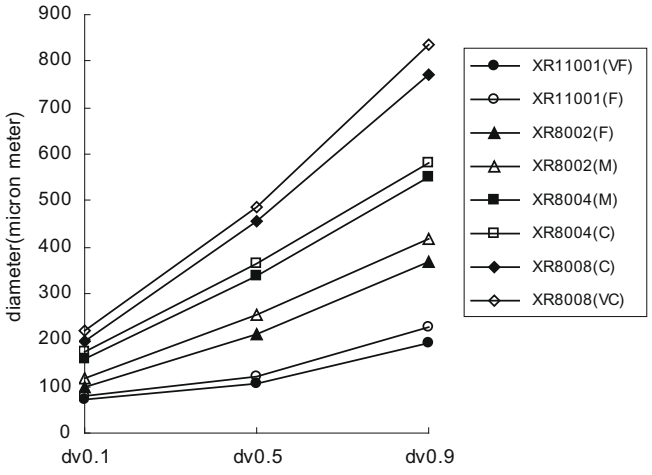

Fig. 15. Nozzle classification result.

the portion of the small droplets in the volume distribution was limited. In these cases, the part in the volume distribution out of the system's capacity could be predicted using the fitted curve. As stated in the Section 4, more works were required to correlate the system with laser-based systems (if possible) or build up its own reference system.

Acknowledgements

The authors express appreciation to Dr. Zhu, Heping, Agricultural Engineer of USDA ARS, to provide data from the Oxford Laser VisiSize system, and Casimiro Gadanha, ESALQ/USP, Piracicaba/Sao Paulo, Brazil, to provide data from the Malvern System.

References

ASAE Standard S-572. 2004. Spray Nozzle Classification by Droplet Spectra.
Benayahu, Y., Ben-David, A., Fastig, S., Cohen, A., 1995. Cloud-droplet size distribution from lidar multiple-scattering measurement. Appl. Opt. 34, 1569–1578.
Berthoumieu, P., Carentz, H., Villedieu, P., Lavergne, G., 1999. Contribution to droplet breakup analysis. Int. J. Heat Fluid Flow 20, 492–498.
Bezdek, J.C., Solomon, K.H., 1983. Upper limit lognormal-distribution for drop size data. J. Irrig. Drain. Eng.-Asce 109, 72–88.
Buchhave, P., Von Benzon, H.-H., 1996. Exploring Pda Configurations. Part. Part. Syst. Charact. 13, 68–78.
Goering, C.E., Bode, L.E., Smith, D.B., 1978. Characterization of spray droplet size distribution. In: First International Conference on Liquid Atomization and Spray Systems. Tokyo, Japan.
Huimin, L., 2000. Science and Engineering of Droplets-Fundamentals and Applications. William Andrew Publishing, Noyes. pp. 397–451 (Chapter 6).
Humeau, Anne, Steenbergen, Wiendelt, Nilsson, Henrik, Strömberg, Tomas, 2007. Laser doppler perfusion monitoring and imaging: novel approaches. Med. Biol. Eng. Comput. 45 (5), 421–435.
Jeon, H.Y., Womac, A.R., Gunn, J., 2004. Sprayer boom dynamic effects on application uniformity. Trans. ASAE 47, 647–658.
Kashdan, J.T., Shrimpton, J.S., Whybrew, A., 2003. Two-phase flow characterization by automated digital image analysis. Part 1: fundamental principles and calibration of the technique. Part. Part. Syst. Charact. 20, 387–397.
Mahler, D.S., Magnus, D.E., 1984. Hot-wire technique for droplet measurements. In: Tishkoff, J.M., Ingelbo, R.D., Kennedy, J.B. (Eds.), Liquid Particle Size Measurement Techniques, ASTM STP 848. American Society for Testing and Materials, pp. 153–165.
Mugele, R.A., Evans, H.D., 1951. Droplet size distribution in sprays. Ind. Eng. Chem. 43, 1317–1324.
Ragucci, R., Cavaliere, A., Massoli, P., 1990. Drop sizing by laser light scattring exploiting intensity angular oscillation in the mie regime. Part. Part. Syst. Charact. 7, 21–25.
Womac, A.R., 2000. Quality control of standardized reference spray nozzles. Trans. ASAE 43, 47–56.
Womac, A., Etheridge, R., Seibert, A., Hogan, D., Ray, S., 2001. Sprayer speed and venturi-nozzle effects on broadcast application uniformity. Trans. ASAE 44 (6), 1437–1444.